

# Hyperspectral Imaging: Wide-Area Spectrophotometry Using a Liquid-Crystal Tunable Filter

ROBERT W. SLAWSON, ZORAN NINKOV, AND ELLIOTT P. HORCH<sup>1</sup>

Center for Imaging Science, Rochester Institute of Technology, 54 Lomb Memorial Drive, Rochester, NY 14623-5604; slawson@cis.rit.edu, ninkov@cis.rit.edu, horch@cis.rit.edu

Received 1998 September 30; accepted 1999 January 19

**ABSTRACT.** This paper reports on the use of a tunable, liquid-crystal filter to obtain simultaneous, low-resolution spectrophotometry of multiple stars within a moderately crowded field. The filter is electronically tunable to any wavelength in the range from 400 to 720 nm with a nominal passband of 10 nm FWHM. In order to evaluate the performance of this filter, the central region of the Jewel Box cluster, NGC 4755, was repeatedly imaged as the filter's central wavelength was stepped from 435 to 720 nm in successive exposures. A spectrum for each of five brighter stars in the cluster field was then reconstructed from the stack of images. Differential corrections for each frame were determined by using a standard spectral scan for one of the stars in the field with a known spectral type (the "reference star"). Dereddened spectra of the other stars in the field were then constructed with accuracy only limited by the match between the reference and standard star spectra, and uncertainties in variable reddening across the cluster. This technique allows multiobject spectroscopy to be obtained in potentially very crowded stellar fields using common photometric reduction techniques—namely, PSF fitting.

## 1. INTRODUCTION

There are a number of approaches to multiobject spectroscopy in astronomy (Walker 1987, pp. 164–177; Taylor 1997). The most enduring is the acquisition of multiple direct images of the same field through a set of glass filters. Such multicolor photometric measurements are essentially very low-resolution spectroscopy, which in the case of the Johnson *UBV* passbands results in a spectral resolution,  $R = \lambda/\Delta\lambda \sim 5$ . The resolution is defined by the bandwidth of the filter and the number of resolution elements by the number of filters. Alternate photometric filter systems (such as *u**b**v*) are also used, although they are less well defined and calibrated. A major difficulty in using fixed filter sets for multiobject spectroscopy is that while increasing the number of filters available (and reducing their passbands) assists in tasks such as spectral classification, it also dramatically increases the difficulties in ease of use, not only in terms of handling but also flat-fielding.

In this paper we demonstrate that low-resolution spectroscopy of multiple point sources in a single field can be extracted from a multispectral series of images obtained with a liquid-crystal tunable filter (LCTF). The demonstration data were obtained of the central region of the "Jewel Box" cluster. A CCD behind the LCTF imaged the open

cluster at 62 different wavelength settings. By performing PSF fitting photometry on each frame in the stack of images and then collecting together the observed fluxes at the various wavelengths for a star, a continuum scan of that star is constructed. This process is shown schematically in Figure 1. The purpose of this paper is to see if such an approach is practical with such a filter and CCD configuration.

Section 2 discusses the operating principle of a liquid-crystal tunable filter. Section 3 details the observations and data reduction. Section 4 discusses the calibration procedure and presents the spectra of 5 of the brighter stars in the field. Finally, § 5 is a summary and some additional remarks.

## 2. THE LIQUID CRYSTAL TUNABLE FILTER

A liquid-crystal tunable filter is essentially a multistage Lyot-Ohman type polarization interference filter (Lyot 1955) with an added liquid-crystal waveplate in each stage providing an electronically controllable variable retardance. As shown schematically in Figure 2*a*, each cell consists of an initial linear polarizer, followed by a birefringent element (quartz) of fixed retardance, then the variable retarder consisting of a liquid crystal waveplate, and a final analyzer oriented with its axis parallel to the initial polarizer. The crystal axis of the quartz retarder is aligned so that

<sup>1</sup> Guest investigator at the University of Toronto Southern Observatory, Las Campanas, Chile.

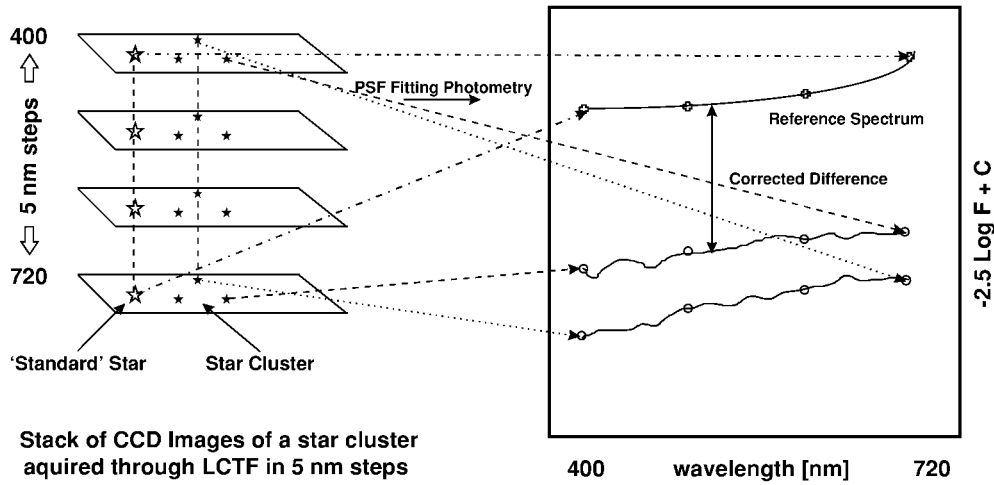


FIG. 1.—Schematic view of the extraction of continuum scans from a hyperspectral stack of cluster images

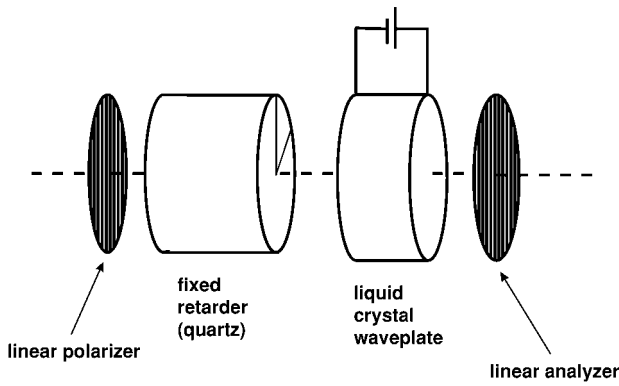


FIG. 2a

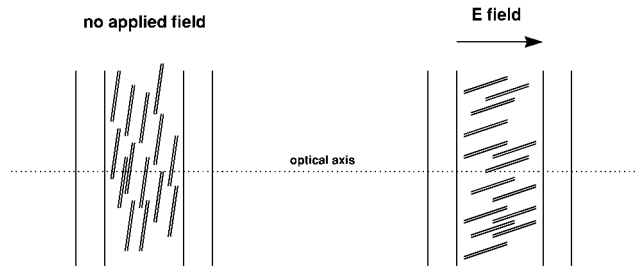


FIG. 2b

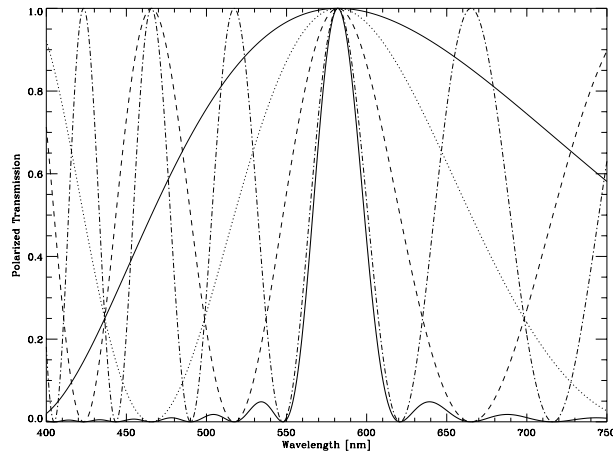


FIG. 2c

FIG. 2.—(a) Schematic diagram of a single Lyot-Ohman cell. (b) Alignment of liquid crystals in the presence of the E-field. (c) Ideal transmittance of a four-stage Lyot-Ohman cell. The bold line is the transmittance through all four stages, which is the product of the transmittances through the individual stages (*lighter weight lines*). Additional stages would narrow the passband and reduce the out-of-band transmission.

the ordinary and extraordinary components of the transmitted light are equal.

The liquid-crystal waveplate consists of two transparent electrodes (indium-tin oxide) on either side of a cell containing nematic liquid crystals. The electrodes are normal to the incident light and the liquid crystals are initially aligned with their long axis nearly perpendicular to the light path (see Fig. 2*b*). The inner surfaces of the cell are prepared in such a way that the molecules have a preferred orientation parallel to the surface (Miller 1991). When a voltage is applied across the electrodes inducing an E-field parallel to the light path, a torque is exerted on the polar, liquid crystal molecules twisting them into the direction of the E-field. The tendency for the molecules to align parallel to the surface provides a restoring force acting against the induced torque such that the amount of twist is proportional to the strength of the field. As the molecules align more closely with the applied field, the retardance through the liquid-crystal waveplate decreases. This produces a waveplate with an electronically adjustable retardance.

A final polarizer selects wavelengths that have undergone an integral  $\pi$  phase shift through the combined quartz and liquid-crystal retarders. This yields a transmittance that varies as  $\cos^2(\delta_\lambda)$ , where  $\delta_\lambda = 2\pi\Gamma/\lambda$  is the phase shift through the combined retarders with total retardance,  $\Gamma$ . A filter consisting of only a single retardance stage, one input polarizer, one quartz retarder, one liquid-crystal waveplate, and a final analyzer would have transmission peaks at wavelengths  $\lambda = 2\Gamma/n, n = 1, 2, 3, \dots$

To isolate a single passband, multiple retardance stages are needed. Stages are placed in series with the retardance of each successive cell increased by a factor of 2. Figure 2*c* shows the (ideal) transmission curves for each of the elements in a four-stage Lyot filter along with the transmission through the stages connected in series. Tuning the filter to a different central wavelength involves changing the retardances of the liquid-crystal waveplates in such a way that the exponential progression in retardance is maintained. A result of this process is that the width of the passband varies across the tunable range approximately as  $\lambda^2$ . Further discussion about LCTF's can be found in Miller (1991).

### 3. OBSERVATION AND DATA REDUCTION

#### 3.1. Observing Details

To evaluate the utility of LCTF devices for multispectral astronomy, a commercial device was used in front of a CCD camera at the University of Toronto's 61 cm telescope on Las Campanas, Chile.

Over three nights in 1997 February, one of us (E. H.) acquired 132 images through an LCTF of the central region of the southern cluster, NGC 4755 (C1250–600, the “Jewel Box”). This is a moderately rich, compact cluster, so named

for its one red ( $\kappa$  Crucis) and four blue supergiants. The cluster also contains numerous candidate pre-main-sequence stars (Dachs & Kaiser 1984; Sagar & Cannon 1995). Figure 3 is an image of the central  $7' \times 7'$  region of NGC 4755 acquired through the LCTF while it was tuned to a central wavelength of 590 nm. The observing conditions during these observations were mostly, but not entirely, photometric.

The LCTF, housed in a  $7.5 \times 7.5 \times 4$  cm aluminum case, is a Cambridge Research & Instrumentation, Inc., Varispec filter model VIS2-10. It was mounted to the front of a Photometrics CH-250 camera housing a Kodak  $2K \times 2K$  CCD using a simple pair of back-to-back adaptor plates. The LCTF has a nominal bandwidth of 10 nm (which varies  $\propto \lambda^2$ ). The central wavelength is tunable to any wavelength between 400 and 720 nm with a setting accuracy of 1 nm or better. The wavelength stability has a temperature coefficient of  $0.22 \text{ nm K}^{-1}$ . An electronic initialization routine effectively removes the temperature dependence at least to first order; it is always performed at start-up and can be reexecuted on demand should the ambient temperature change significantly during the night.

The transmittance of the LCTF varies from 31% at the red end (720 nm) decreasing to 5% at 435 nm for *randomly* polarized incident light. Table 1 lists measured transmittances for randomly polarized light through the filter at a representative set of wavelengths. For linearly polarized light, the transmittances are twice these values. Most of the variation is attributable to the increase in absorption of the ITO electrodes, particularly at the shorter wavelengths.



FIG. 3.—150 s exposure of NGC 4755 (C1250–600) with the LCTF tuned to a center wavelength of 590 nm. The passband of the LCTF is fixed at 10 nm.

TABLE 1  
TRANSMITTANCES THROUGH THE LCTF  
FOR RANDOMLY POLARIZED,  
INCIDENT LIGHT

$\lambda$ (nm)	$T$ (%)	$\lambda$ (nm)	$T$ (%)
440.....	6	600.....	20
480.....	13	640.....	22
520.....	18	680.....	27
560.....	19	720.....	31

NOTE.—Transmittances of linearly polarized light are 2 times the above values.

This filter is the high-contrast version with less than 0.01% out-of-band transmission within 400–720 nm. In addition, a hot mirror (high-pass filter) is placed ahead of the filter to remove near-IR leakage. The LCTF has a circular clear aperture of 35 mm and a field of view of  $\pm 7^\circ$  from the normal. In the worst case, at the largest incident angle, the wavelength shift is less than 1 nm; for the outside edge of an  $f/15$  telescope beam, as at the UTSO 61 cm, the wavelength shift is even smaller (CRI Tech Note VS-001). At a filter temperature of 25 C the time to alter the wavelength setting is  $\sim 50$  ms, although taking longer at lower temperatures.

The camera head used with the LCTF contains a thermoelectrically cooled Kodak KAF-4200  $2K \times 2K$  CCD (useful area  $2030 \times 2042$  pixels) with  $9 \mu\text{m}$  square pixels. At the focal plane scale of the UTSO 61 cm telescope, the field of view of the CCD is  $\sim 7'$  on a side and in typical seeing the FWHM of the stellar PSF is 5–7 pixels. The CCD is read out at 200 kHz, requiring  $\sim 21$  s to read the entire array, and has a rms read noise of  $11 e^-$ . There was no measurable vignetting from the 35 mm circular aperture of the LCTF.

Operation of the filter requires that an additional cable and small control box be placed relatively close to the unit ( $< 2$  m) but communication between the control box and the data computer (or a hand paddle controller) is via a standard serial line allowing for much larger separations. This lightweight, compact system was then attached to the instrument mounting plate of the UTSO's guided direct camera.

The images were mostly acquired with the filter's center wavelength incremented in 5 nm steps across the wavelength range 435–720 nm. Usually two exposures, differing in exposure time by a factor of 10, were obtained at each wavelength setting of the LCTF. The exposure times ranged between 25 and 600 s, with the longer exposures at the bluest wavelengths. Smaller wavelength steps of 2–3 nm were taken near the  $H\alpha$  and  $H\beta$  lines. Steps of 10 nm would be adequate for these observations; however, at the time the observations were acquired, it was believed that this filter

had a 5 nm passband. Subsequent investigation revealed that it was in fact 10 nm wide.

Dome flats were acquired for flat-fielding purposes at 50 nm intervals from 450 to 700 nm inclusive with the intent that the flat-field image nearest in wavelength to the object image would be used for correcting it. This procedure should be satisfactory unless there are rapid changes in the pixel quantum efficiencies with wavelength across the array, which is known not to be the case.

### 3.2. Data Reduction

The images were processed using the standard IRAF CCD processing pipeline and were trimmed, bias subtracted, and flat-fielded. The flat-field image used was that closest in wavelength from the series of dome flat images. All the frames were registered and transformations from the individual frame pixel coordinates to a common pixel coordinate system were determined and applied. All the frames could then be stacked (conceptually) into a data cube with axes consisting of  $X$ - $Y$  position (image) and wavelength (spectra) sorted into order as shown in Figure 1.

Point spread function fitting photometry of the stars in each frame was carried out using the IRAF implementation of DAOPHOT, and aperture corrections were applied to the resulting instrumental magnitudes. Much of this procedure was automated using scripts.

The standard deviation of the repeated measurements indicates a photometric uncertainty of 0.02–0.03 mag. The largest contribution to this uncertainty appears to be from the flat-field corrections, at least for the bright stars presented here. The dome flats acquired for these observations may be less than optimal and have an estimated error of  $\sim 1.4\%$ . Moreover, no fringing from the filter itself was noted in the flat-field frames at any wavelength.

Previous studies of this cluster have reported that the reddening is somewhat variable across this cluster. In particular, Dachs & Kaiser (1984) found that  $E_{B-V}$  varies by 0.08 mag across an  $18'$  field but the variation is only 0.03 mag across the central  $6'$  region, which is only slightly smaller than our CCD field. Such small variations in the reddening, which have not been corrected for in this work, will have only a minor effect on the spectra presented.

## 4. DEMONSTRATION

The photometric data for each star from each frame can then be assembled into a set of raw spectra. Variations in the sky transparency and extinction due to hour angle changes requires that the instrumental magnitudes from each frame be normalized to some reference. The procedure followed here is to adopt, as the reference, a single star measurable on all the images obtained whose spectral type was known. A previously obtained absolute spectrum of

this star could then be used to obtain normalizing coefficients between the raw and reference spectra. Once the coefficients were available, they could then be used to normalize all the raw spectra obtained.

To test this concept the field of the Jewel Box cluster was observed. This choice was made because the field contains a number of stars for which spectral types have been previously determined. It was therefore possible to select a star as the reference and determine how well the spectra for other stars compared to the spectral types in the literature. To this end, the stars listed in Table 2, and identified by their Arp & van Sant (1958) designation, were used. These stars are also marked on the image of the cluster (Fig. 3).

The star I-15, which had a measurable flux in every image, was selected as the spectral reference for the cluster. This star has a known spectral type, B1 V (Feast 1963). The absolute spectrum of this star was taken to be the same as that of the B1 V spectrum of BD -1 935 tabulated in the spectrophotometric atlas of Gunn & Stryker (1983). They provide no special remarks about this spectrum, and we therefore assume it is typical of that class.

The spectrum of BD -1 935 from Gunn & Stryker was spline fitted, rebinned, and convolved with a 10 nm FWHM  $\cos^2(\delta)$  function that provides the shape and nominal width of the LCTF passband. That is, the spectrum was degraded from the 1-2 nm resolution of Gunn & Stryker's atlas to the 10 nm resolution of the LCTF. For each CCD frame, the difference in magnitudes between the value measured for star I-15 and the value of the prepared standard spectrum at the wavelength of the frame was computed and applied to all the other stars in that frame as a zero-point correction.

To the extent that the spectrum of BD -1 935 accurately represents the intrinsic spectrum of star I-15, this procedure removes the instrumental response, atmospheric absorption, and the effect of foreground interstellar reddening from the data. However, any difference between the spectrum of BD -1 935 and true spectrum of I-15 at a particular wavelength will also be present in the corrected spectra of all the other stars in the frame on which the offset correction is applied.

Figure 4 shows four calibrated spectra of the bright cluster stars D, I-5, III-6, and one nonmember (superimposed on the core region of the cluster), I-4, as extracted from the data cube in the manner described. Most of the plotted points are the mean corrected fluxes from at least two separate CCD frames. The plotting symbols used in Figure 4 are  $\pm 0.03$  mag in extent. The zero point for the

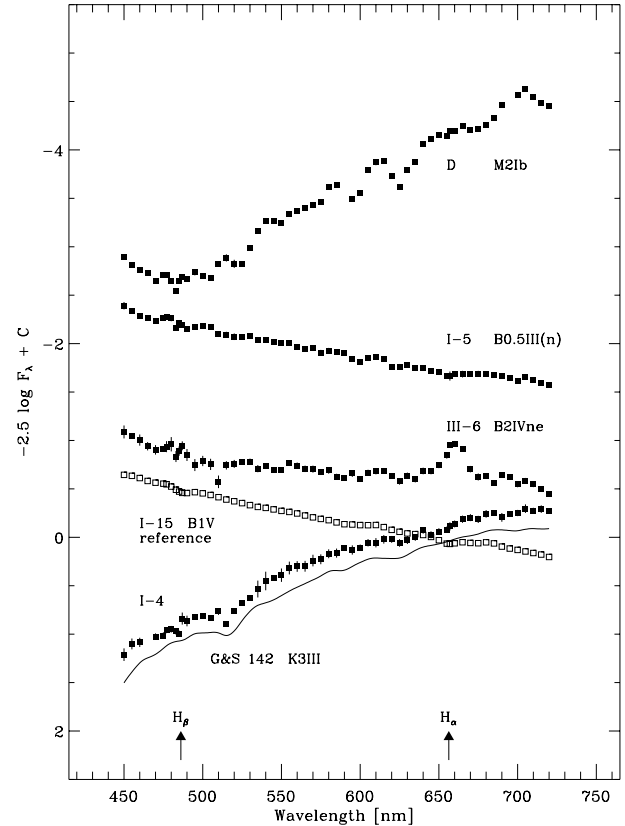


FIG. 4.—Extracted continuum scans of stars D, I-5, III-6, I-4, and the reference star, I-15. A spectrophotometric scan of a K3 III from Gunn & Stryker (1983) is shown next to the observed spectrum of I-4 indicating a spectral type match for this star. The spectrum of I-15 is the spectrum of BD -1 935 from Gunn & Stryker at the resolution of the LCTF: we have assumed they are identical.

TABLE 2  
SOME PARAMETERS OF OBSERVED STARS

ID	Spectral Type	V	B - V	U - B	Notes
D .....	M2 Ib	7.42	2.19	2.38	
I-5 .....	B0.5 III(n)	8.61	0.16	-0.70	
III-6 .....	B2 IVne	9.88	0.22	-0.65	
I-4 .....	K3 III <sup>a</sup>	11.03	1.57	1.39	Nonmember
I-15 .....	B1 V	10.24	0.14	-0.58	Local reference

NOTES.—Spectral types (other than for I-4) are from Feast 1963, except for III-6, which is from Schild 1970. V, B - V, and U - B are from Perry et al. 1976, except for I-4, which is from Dachs & Kaiser 1984.

<sup>a</sup> Determined in this paper; see § 4.

magnitude scale was set to the observed flux at 555 nm of the reference star, I-15. (The spectrum of I-15 shown in the figure is the same as the prepared spectrum of BD -1 935: we assumed they are identical).

The derived spectra in Figure 4 show the features expected for their listed spectral types. For example, in the spectrum of the known M2 supergiant, star D, several broad molecular absorption bands of TiO are evident (band heads at 665, 616, 585, 517, and 495 nm). Strong emission in the H $\alpha$  line (656 nm) can be seen in the spectrum of star III-6, a known emission-line star. And the continuum of I-5, a B0.5 III star, is fairly featureless, as expected at this resolution.

Plotted just below the scan of star I-4, which does not have a spectral type reported in the literature, is the spectrum of HD 83618 from Gunn & Stryker (1983), which has a spectral type of K3 III. The resolution of this spectrum was degraded to that of the LCTF by exactly the same procedure described previously. This spectrum, of those in the Gunn & Stryker atlas, has the best (by eye) match to the shape and features of the observed spectrum of I-4. The most obvious feature is the Mg b triplet, centered at 513 nm, which matches the K3 III scan rather well in depth. Even some of the minor features in the K3 III scan match those in star I-4. We also note that the observed colors (Table 2) for star I-4 are consistent with a moderately reddened early K giant.

## 5. SUMMARY AND REMARKS

A new approach to obtaining multiobject spectrophotometry using a tunable liquid-crystal filter in front of a CCD camera has been demonstrated. For demonstration purposes, multiple images of the central region of the open cluster NGC 4755 were acquired through the filter and magnitudes were measured for all stars in the images with PSF fitting photometry. A simple calibration was adopted by assuming that a spectrophotometric scan from an atlas matched the intrinsic spectrum of a cluster star with the same spectral class. A differential correction was computed between the atlas scan and the measured magnitudes for

this star, and then applied to all the other stars on a frame-by-frame basis. Spectra for four stars were extracted from the data set to demonstrate that broad features, such as molecular bands, are detectable as well as the overall shape (slope) of the continuum.

Using this approach, very low-resolution spectroscopic information should be obtainable in any field where image processing techniques can be used to extract photometric data. This might be of particular advantage in dense fields where crowded field techniques, such as PSF fitting, could yield spectrophotometry for many hundreds of objects. In contrast, techniques for multiobject spectroscopy that use fibers or use multislit masks are limited by a minimum separation between selected objects and cannot observe all the objects in a crowded field.

In the future, we intend to observe older clusters where later type stars with broad molecular bands are more abundant. Since such clusters are also generally free of dust, differential reddening is no longer a problem. At worst, any reddening arises from foreground dust and is essentially uniform across the cluster. With the differential spectrophotometric approach followed here, the reddening cancels out. We also intend to explore objective spectral classifications by, for example, cross-correlation of observed scans against a suitable standard grid. Other observational projects include two-dimensional spectrophotometric imaging of young star-forming regions and emission nebulae. Some images have already been obtained (Ninkov, Bretz, & Tang 1997), and more are planned. In addition, a significant improvement in the data quality will come with the use of a thinned, back-illuminated CCD whose better blue response offsets the lower transmission of the filter at shorter wavelengths.

We thank Barry Logue of Cambridge Research & Instrumentation for information on the LCTF. We also thank the (now closed) University of Toronto Southern Observatory for observing time. An anonymous referee provided a critique that led to an improved paper. This work was supported by funding for detector development from the NSF S/IUCRC program and the New York State CAT program.

## REFERENCES

- Arp, H. C., & Van Sant, C. T. 1958, *AJ*, 63, 341  
 Dachs, J., & Kaiser, D. 1984, *A&AS*, 58, 411  
 Feast, M. W. 1963, *MNRAS*, 126, 11  
 Gunn, J. E., & Stryker, L. L. 1983, *ApJS*, 52, 121  
 Lyot, B. 1955, US Patent 2, 718, 170  
 Miller, P. J. 1991, *Metrologia*, 28, 145  
 Ninkov, Z., Bretz, D., & Tang, C. 1997, *Laser Focus*, 33, 141  
 Perry, C. L. et al. 1976, *AJ*, 81, 632  
 Sagar, R., & Cannon, R. D. 1995, *A&AS*, 111, 75  
 Schild, R. E. 1970, *AJ*, 161, 855  
 Taylor, K. 1997, in *Instrumentation for Large Telescopes*, ed. J. M. R. Espinosa, A. Herrero, & F. Sánchez (Cambridge: Cambridge Univ. Press), 134  
 Walker, G. W. 1987, *Astronomical Observations* (Cambridge: Cambridge Univ. Press)